IOP Conf. Series: Journal of Physics: Conf. Series **1356** (2019) 012022 doi:10.1088/1742-6596/1356/1/012022

Verification of Floating Offshore Wind Linearization Functionality in OpenFAST

N Johnson[1], J Jonkman[2], A Wright [3], G Hayman[4], and A Robertson[5]

[1] Research Engineer, National Renewable Energy Laboratory, Golden, Colorado, USA
[2] Senior Research Engineer, National Renewable Energy Laboratory, Golden, Colorado, USA
[3] Senior Research Engineer, National Renewable Energy Laboratory, Golden, Colorado, USA
[4] Consultant, Boulder, Colorado, USA
[5] Senior Research Engineer, National Renewable Energy Laboratory, Golden, Colorado, USA

E-mail: nick.johnson@nrel.gov

Abstract. The wind engineering community relies on multiphysics engineering software to run nonlinear time-domain simulations, e.g., for design standards-based loads analysis. Although most physics involved in wind energy are nonlinear, linearization of the underlying nonlinear system equations is often advantageous to understand the system properties and exploit well-established methods and tools for analyzing linear systems. Previous work in this area has focused on the development of the new linearization functionality of the open-source engineering tool OpenFAST for floating offshore wind turbines, as well as the concepts and mathematical background needed to understand and apply it correctly. This paper focuses on the verification of this new linearization functionality, which is carried out by comparing results to previous stable versions of FAST. A nonlinear time-domain simulation for a floating offshore platform is also compared to the time-domain response of the linearized state-space model. The linearized results show good alignment between OpenFAST and previous versions of FAST, as well as with the time-domain simulations, thereby showing the accuracy of the new features in OpenFAST.

1. Introduction

OpenFAST (formerly known as FAST), developed by the National Renewable Energy Laboratory (NREL), is a coupled aero-hydro-servo-elastic analysis tool for modeling floating offshore wind turbines. The primary use of OpenFAST is to run nonlinear time-domain simulations (e.g., for design standards-based loads analysis). Although most physics involved in wind energy are nonlinear, linearization of the underlying nonlinear system equations is often advantageous to understand the system response and exploit well-established methods and tools for analyzing linear systems. The ability to generate linearized models is important for eigenanalysis (to derive structural natural frequencies, damping ratios, and mode shapes), controls design (based on linear state-space models), stability analysis, gradients for optimization problems, and support

for the development of reduced-order models. The linearization functionality of OpenFAST was recently extended to floating offshore wind turbines, including the hydrodynamics, moorings, and their coupling to the wind turbine. The theoretical details of the linearization process have been published previously [1]. This paper will verify the validity of the linear solution when compared to that of the nonlinear time-domain solution and will show that the new functionality yields results in alignment with past versions of FAST. A state-space wave-excitation model used in the linearization analysis and updates to the multiblade coordinate transformation utility for three-bladed wind turbines (MBC3) necessary for offshore linearization analysis are provided in this paper.

The approach for verification is to compare the linearization results produced by OpenFAST, which includes new features, and the results produced by FAST v7. FAST v7 was selected as a benchmark because it is the most recent version of FAST to include hydrodynamics in the linearization process; however, it should be noted that FAST v7 does not include the wave-radiation or wave-excitation terms that have been added to the linearization of OpenFAST. The linearization results include natural frequencies and damping ratios of the blades, tower, and platform degrees of freedom. Three cases were considered in the verification: an OpenFAST and FAST v7 generated Campbell diagram of the OC3 Hywind-spar as a function of rotor speed (without aerodynamics), an OpenFAST and FAST v7 generated Campbell diagram of the OC3 Hywind-spar as a function of wind speed (with aerodynamics), and an OpenFAST time-domain simulation of the Offshore Code Comparison Collaboration Continuation (OC4)-DeepCwind semisubmersible with both the linear and nonlinear models. The verification process increases in complexity with each case to isolate any unexpected behavior, and to ensure that all of the capabilities are fully functional and verified.

2. Linearization

The OpenFAST linearization process involves defining an operating point, linearizing the underlying nonlinear equations of each module about the operating point, linearizing the module-to-module input-output coupling relationships about the operating point, and combining all linearized matrices into the full-system, linear state-space model. The new linearization functionality enables the contributions from state-space-based wave excitation, hydrodynamic added mass, state-space-based wave-radiation damping, hydrostatic restoring, linearized viscous drag, and linearized mooring restoring for a floating offshore wind turbine to be included in the full linearized system (along with linearization of the wind turbine structure, aerodynamics, and controller). The new linear state-space-based wave excitation and wave-radiation damping offset the use of discrete Fourier transforms and numerical convolution typically used for nonlinear time-domain simulations, respectively, but that are not conducive to linearization. See [1] for the theoretical details of the linearization process.

3. Updates to MBC3

MBC3 [2] is an analysis tool for modal and stability analysis for a wind turbine with a spinning three-bladed rotor that converts the rotating inputs, outputs, and states to a fixed, nonrotating frame. Once all of the states are in the same frame, an eigenanalysis can be performed, and modal analysis can be completed. Before the addition of hydrodynamic states, whose state equations only involve first-time derivatives, MBC3 previously applied only to a set of states whose state equations involved second-time derivatives. This section documents the updates to

the MBC3 theory basis to include the hydrodynamic states added to the linearization process.

Equations from [2] will be referred to with an asterisk. Some new notation is also included here to correspond with the notation in other FAST/OpenFAST-related linearization documents (i.e., z becomes Δx, u becomes Δu, X becomes Δq_2, and Y becomes Δy). Additionally, w has been eliminated because the disturbance terms have been combined with the control inputs in FAST/OpenFAST.

Here we define a new state variable that only applies to first-order systems (i.e., the HydroDyn states), Δq_1. The state vector x, in equation 26*, is now given by:

$$\Delta x = \begin{Bmatrix} \Delta q_2 \\ \Delta \dot{q}_2 \\ \Delta q_1 \end{Bmatrix} \tag{1}$$

and,

$$\Delta \dot{x} = \begin{Bmatrix} \Delta \dot{q}_2 \\ \Delta \ddot{q}_2 \\ \Delta \dot{q}_1 \end{Bmatrix} \tag{2}$$

and from equation 10* and 13*,

$$\Delta q_1 = T_{1q} \Delta q_{1_{NR}} \tag{3}$$
$$\Delta \dot{q}_1 = T_{1q} \Delta \dot{q}_{1_{NR}} + \Omega T_{2q} \Delta q_{1_{NR}} \tag{4}$$

and,

$$\Delta q_2 = T_1 \Delta q_{2_{NR}} \tag{5}$$
$$\Delta \dot{q}_2 = T_1 \Delta \dot{q}_{2_{NR}} + \Omega T_2 \Delta q_{2_{NR}} \tag{6}$$
$$\Delta \ddot{q}_2 = T_1 \Delta \ddot{q}_{2_{NR}} + 2\Omega T_2 \Delta \dot{q}_{2_{NR}} + (\Omega^2 T_3 + \dot{\Omega} T_2) \Delta q_{2_{NR}} \tag{7}$$

The transformation matrix for q_1 is given by

$$T_{1q} = \begin{bmatrix} I_{F_{q1} \times F_{q1}} & & & & & \\ & \tilde{t} & & & & \\ & & \tilde{t} & & & \\ & & & \tilde{t} & & \\ & & & & \ddots & \\ & & & & & \tilde{t} \end{bmatrix}_{(F_{q1}+3m_{q1}) \times (F_{q1}+3m_{q1})} \tag{8}$$

and likewise,

$$T_{2q} = \begin{bmatrix} 0_{F_{q1}\times F_{q1}} & & & & & \\ & \tilde{t_2} & & & & \\ & & \tilde{t_2} & & & \\ & & & \tilde{t_2} & & \\ & & & & \ddots & \\ & & & & & \tilde{t_2} \end{bmatrix}_{(F_{q_1}+3m_{q_1})\times(F_{q_1}+3m_{q_1})} \tag{9}$$

Where F_{q1} and m_{q1} are the number of first-order states in the fixed and rotating frames, respectively. Note that $F_{q1} + m_{q1}$ equals the total number of first-order states. Using the new nomenclature, equation 24* now becomes,

$$\Delta\dot{x} = A\Delta x + B\Delta u \tag{10}$$

and equation 25* becomes,

$$\Delta y = C\Delta x + D\Delta u \tag{11}$$

Substituting equation 1 and equation 2 into equation 10, we find,

$$\begin{Bmatrix} \Delta\dot{q_2} \\ \Delta\ddot{q_2} \\ \Delta\dot{q_1} \end{Bmatrix} = A \begin{Bmatrix} \Delta q_2 \\ \Delta\dot{q_2} \\ \Delta q_1 \end{Bmatrix} + B\Delta u \tag{12}$$

Where equation 20* becomes,

$$\Delta u = T_{1C}\Delta u_{NR} \tag{13}$$

This yields the following expressions for the state matrices in the nonrotating frame, replacing equations 29* and 30*:

$$A_{NR} = \begin{bmatrix} T_1^{-1} & 0 & 0 \\ 0 & T_1^{-1} & 0 \\ 0 & 0 & T_{1q}^{-1} \end{bmatrix} \left\{ A \begin{bmatrix} T_1 & 0 & 0 \\ \Omega T_2 & T_1 & 0 \\ 0 & 0 & T_{1q} \end{bmatrix} - \begin{bmatrix} \Omega T_2 & 0 & 0 \\ \Omega^2 T_3 + \dot{\Omega} T_2 & 2\Omega T_2 & 0 \\ 0 & 0 & \Omega T_{2q} \end{bmatrix} \right\} \tag{14}$$

$$B_{NR} = \begin{bmatrix} T_1^{-1} & 0 & 0 \\ 0 & T_1^{-1} & 0 \\ 0 & 0 & T_{1q}^{-1} \end{bmatrix} BT_{1C} \tag{15}$$

Subsituting equation 1 and equation 22* into output equation 11 becomes,

$$Y_{NR} = T_{1O}^{-1} \left[C \begin{Bmatrix} T_1\Delta q_{2_{NR}} \\ T_1\Delta\dot{q_2} + \Omega T_2\Delta q_{2_{NR}} \\ T_{1q}\Delta q_{1_{NR}} \end{Bmatrix} + DT_{1C}\Delta u_{NR} \right] \tag{16}$$

Therefore, equation 31* becomes,

$$C_{NR} = T_{1O}^{-1}\left[C_d T_1 + \Omega C_v T_2 \quad C_v T_1 \quad C_q T_{1q}\right]; \quad C = \begin{bmatrix} C_d & C_v & C_q \end{bmatrix} \tag{17}$$

Where C_q is the damping matrix associated with the HydroDyn states.

4. Campbell Diagrams

A series of simulations were run to highlight the functionality and verify the implementation of the new OpenFAST linearization capability for offshore wind systems. First, the NREL 5-MW baseline wind turbine atop the OC3-Hywind spar buoy [3] was run with the following conditions: still water, no wind inflow, no aerodynamic forcing, no pitch control, and no torque control. The natural frequencies and damping were calculated with the linearized model as a function of rotational speed and presented in Campbell-diagram form.

To compute the full-system natural frequencies of the NREL 5-MW baseline turbine in OpenFAST and FAST v7, as a function of rotor speed in the absence of aerodynamic loading, the ElastoDyn, ServoDyn, HydroDyn, and MAP++ modules were enabled and the InflowWind and AeroDyn modules were disabled. All pertinent structural degrees of freedom were enabled in the ElastoDyn module, including blade-bending, drivetrain-torsion, generator-rotation, nacelle-yaw, tower-bending, and floating platform translation. Additionally, rotation degrees of freedom and gravitational loading, structural (but no aerodynamic) damping, mooring restoring, and hydrodynamic added mass, radiation and viscous damping, and hydrostatic restoring were included. The ServoDyn module provided nacelle-yaw actuator stiffness and damping. A separate linearization analysis was run at each rotor speed from 0 to 14 rpm, in steps of 2 rpm. The rotor-collective blade-pitch angles were fixed at 0°. For each rotor speed, a periodic steady-state condition is found by marching the nonlinear solution in time long enough for start-up transients to die out (the start-up transients exist because gravity and rotor rotation have an influence on the structural displacements, which are assumed undisplaced at time zero, and die out as a result of structural and hydrodynamic damping). After a periodic steady-state condition was reached, one more rotor revolution (360°) was simulated, and an operation point was set and the linearized full-system state matrix (A) is computed for each azimuth angle of the rotor in 36 steps of 10°. MBC3 was used to read-in the periodic state matrices; apply the MBC transformation to the rotating states to transform them to states in the fixed frame; azimuth-average the MBC-transformed state matrices; compute the eigensolution of the resulting azimuth-averaged matrix; and extract the natural (undamped) frequencies and damping ratios from this eigensolution. Results for the natural frequencies from OpenFAST are shown in Figure 1.

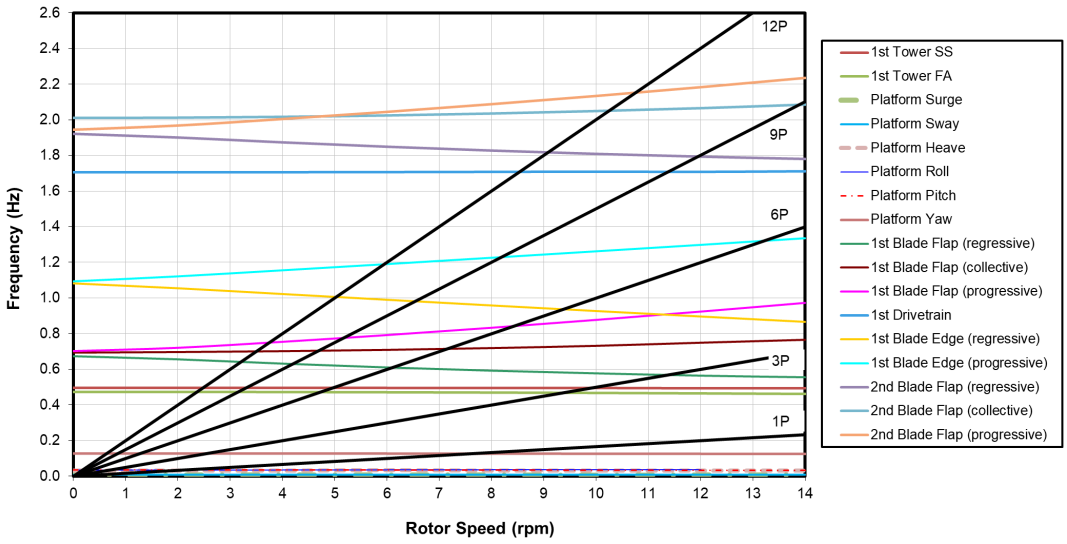

Figure 1: Campbell diagram as a function of rpm for OpenFAST

This result is in almost perfect alignment with those from FAST v7, so the latter are not shown. The results for the damping ratios are shown in Figure 2 for OpenFAST and for FAST v7.

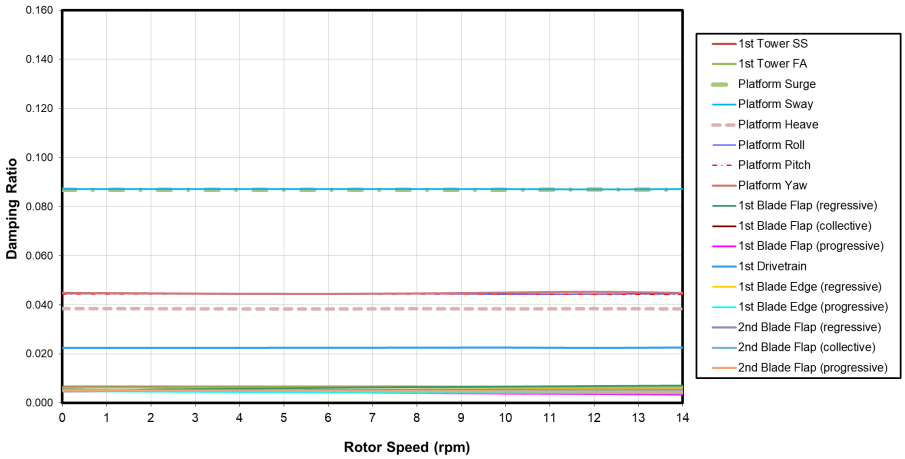

(a) OpenFAST

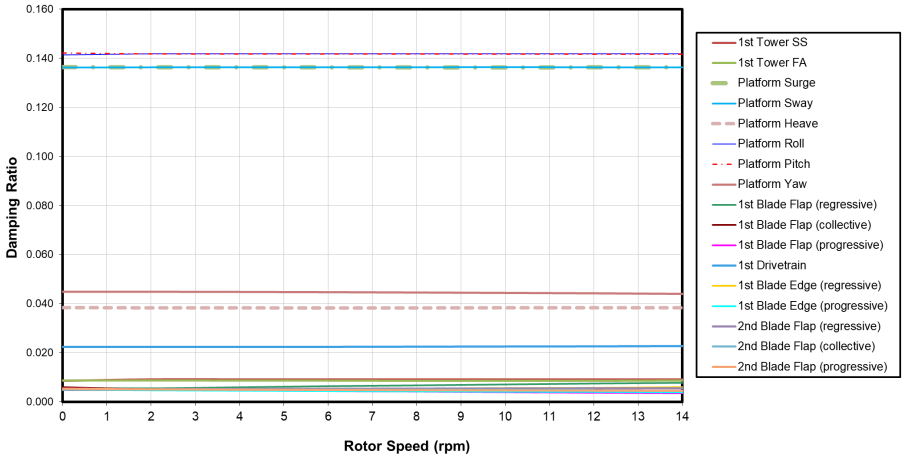

(b) FAST v7

Figure 2: Damping ratios as a function of rpm for (a) OpenFAST and (b) FAST v7

The damping of the floating platform modes differs a bit between OpenFAST and FAST v7. This is a result of two factors. First, radiation damping could not be linearized in FAST v7 and so was neglected in the linearization process (that said, the radiation damping is small for the OC3-Hywind spar). Second, the linearization of the viscous-drag term is sensitive to the perturbation size at the operating point condition used in this case (where the operation point velocity is zero because the spar is in static equilibrium when linearized). FAST v7 and OpenFAST predict slightly different amounts of damping because their perturbation sizes differ. The basic problem is that the viscous-drag term cannot be properly linearized with a perturbation technique (there are other linearization approaches, such as stochastic linearization, but these are outside the scope of this project).

The damping ratios for the blades and tower are a good fit between OpenFAST and FAST v7. Figure 3 shows an enlarged view of the blade and tower damping ratios to more easily see the details. We can see that the same general trends exist for the blade and tower damping. Therefore, we believe that the fit between the OpenFAST and FAST v7 is good and the result

from OpenFAST is reliable.

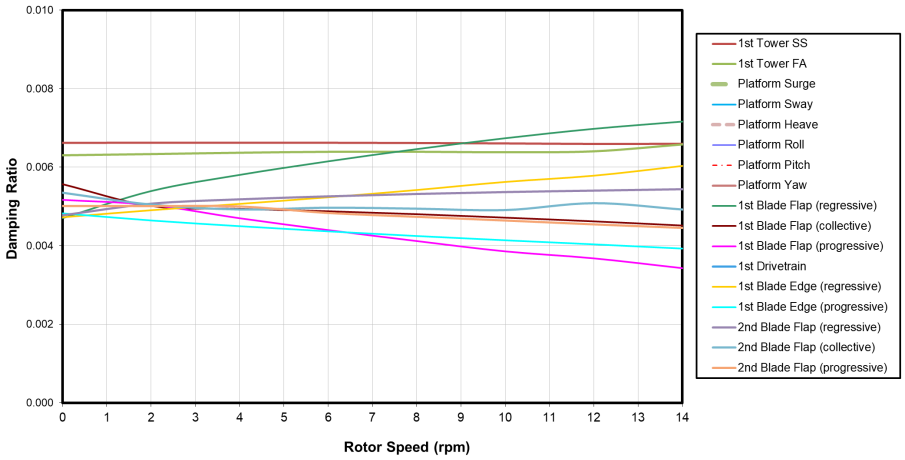

(a) OpenFAST

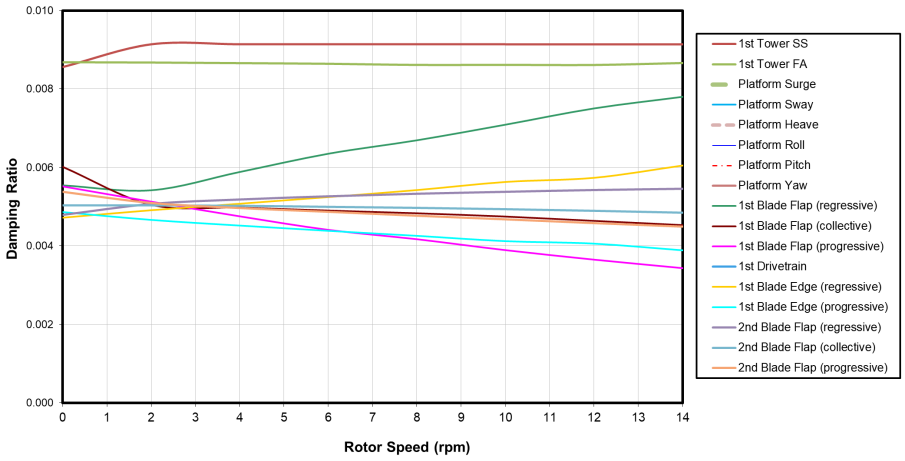

(b) FAST v7

Figure 3: Detailed damping ratios as a function of rpm for (a) OpenFAST and (b) FAST v7

For the next verification test, the following conditions were used: still water, wind inflow enabled, aerodynamic forcing enabled, and fixed pitch and torque. The natural frequencies and damping were calculated with the linearized model as a function of mean hub-height wind speed.

The full-system natural frequencies of the NREL 5-MW baseline turbine, in OpenFAST and FAST v7, were computed as a function of mean hub-height wind speed. ElastoDyn, ServoDyn, HydroDyn, MAP++, InflowWind, and AeroDyn modules were enabled. All pertinent structural degrees of freedom were enabled in the ElastoDyn module including blade-bending, drivetrain-torsion, generator-rotation, nacelle-yaw, tower-bending, and floating platform translation. Additionally, rotation degrees of freedom and gravitational loading, structural and aerodynamic damping, mooring restoring, and hydrodynamic added mass, radiation and viscous damping, and hydrostatic restoring were included. The ServoDyn module provided nacelle-yaw actuator stiffness and damping. A separate linearization analysis was run at each mean hub-height wind

speed from 3 to 25 meters per second, in steps of 1 meter per second. The rotor-collective blade-pitch angles were fixed at 0° for below rated, and they follow a pitch-speed curve above rated. The generator torque was also set appropriately to each wind speed following a torque-speed curve, resulting in variable rotor speed below rated and fixed rotor speed above rated. For each wind speed, a periodic steady-state condition was found by marching the nonlinear solution in time long enough for start-up transients to die out (the start-up transients exist because gravity, rotor rotation, and aerodynamic loads have an influence on the structural displacements, which are assumed undisplaced at time zero, and die out as a result of structural, hydrodynamic, and aerodynamic damping). After a periodic steady-state condition is reached, one more rotor revolution (360°) was simulated, and an operation point was set and the linearized full-system state matrix (A) was computed for each azimuth angle of the rotor in 36 steps of 10°. MBC3 was used to read-in the periodic state matrices; apply the multiblade coordinate transformation to the rotating states to transform them to states in the fixed frame; azimuth-average the multiblade coordinate-transformed state matrices; compute the eigensolution of the resulting azimuth-averaged matrix; and extract the natural (undamped) frequencies and damping ratios from this eigensolution. Results for the natural frequencies from OpenFAST and FAST v7 are shown in Figure 4.

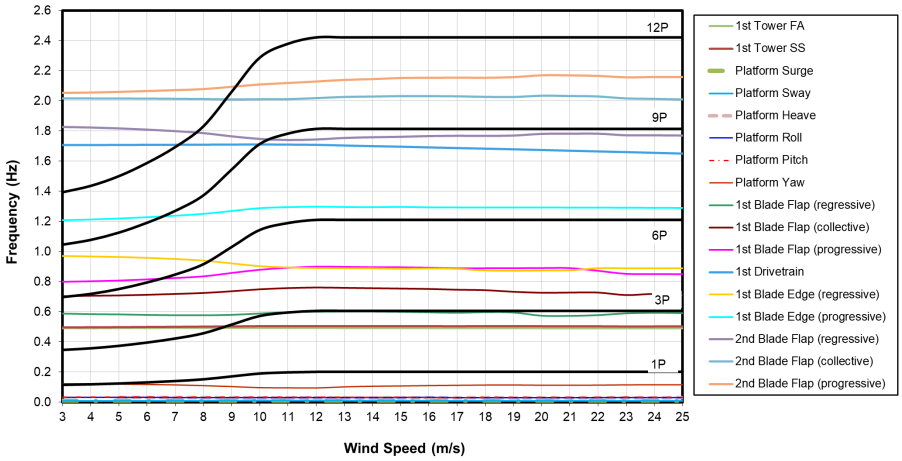

(a) OpenFAST

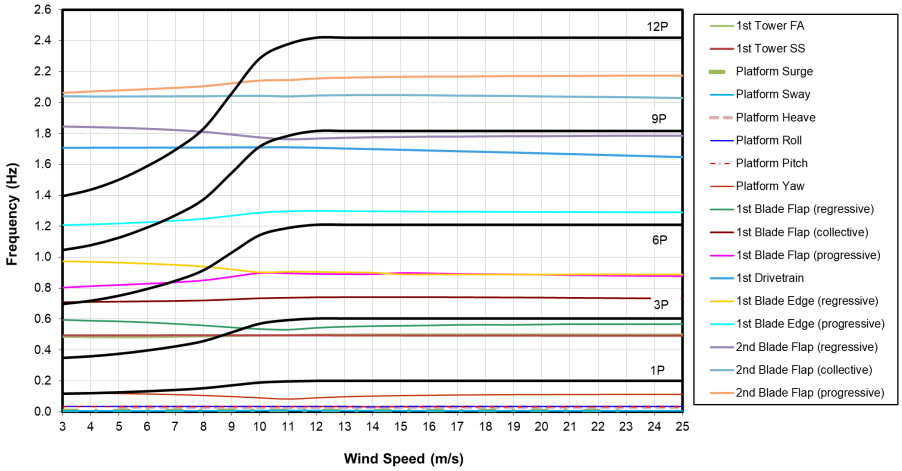

(b) FAST v7

Figure 4: Campbell diagram as a function of wind speed for (a) OpenFAST and (b) FAST v7

Overall, the natural frequencies for OpenFAST match that of FAST v7. There are a few discrepancies, however. The results from OpenFAST are not as smooth as the results from FAST v7. The biggest reason for this is because a steady-state trim calculation (referred to as CalcStdy) is not currently available in OpenFAST. This feature is available in FAST v7 and involves varying one control input based on a proportional feedback control law to achieve a desired rotor speed while holding other control inputs fixed. The simulation ends when a steady solution is found. This is determined by a 2-norm of the differences between conditions at the beginning and end of the iteration is computed [4]. In lieu of the CalcStdy function, simulations in OpenFAST were run by prescribing fixed pitch and torque values and simulating until they reached steady state (>1300 seconds). Another complicating factor is that the pitch and generator torque settings for the NREL 5 MW [5] were developed with FAST v7 and were not tuned for OpenFAST. An iterative interpolation was necessary to tune the generator torque to get the correct rotor speed, but some of the rotor speeds were not completely the same as those in FAST v7 simulations, thus causing a difference.

The results for the damping ratios are shown in Figure 5 for OpenFAST and for FAST v7.

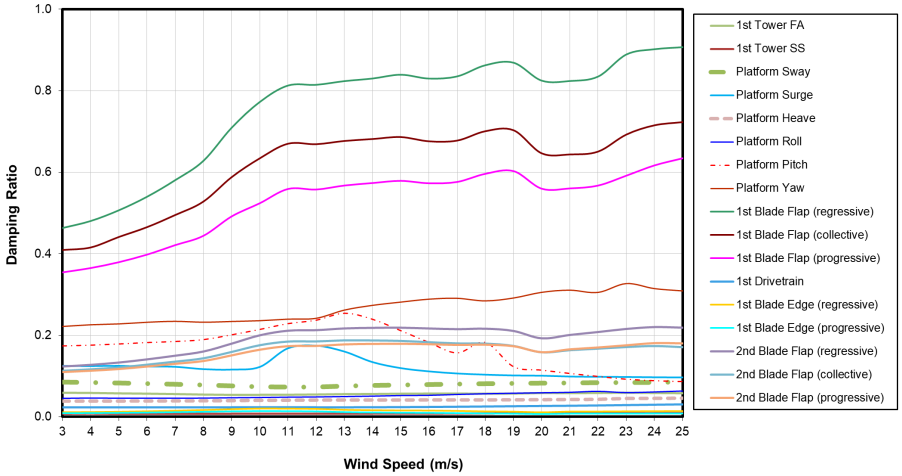

(a) OpenFAST

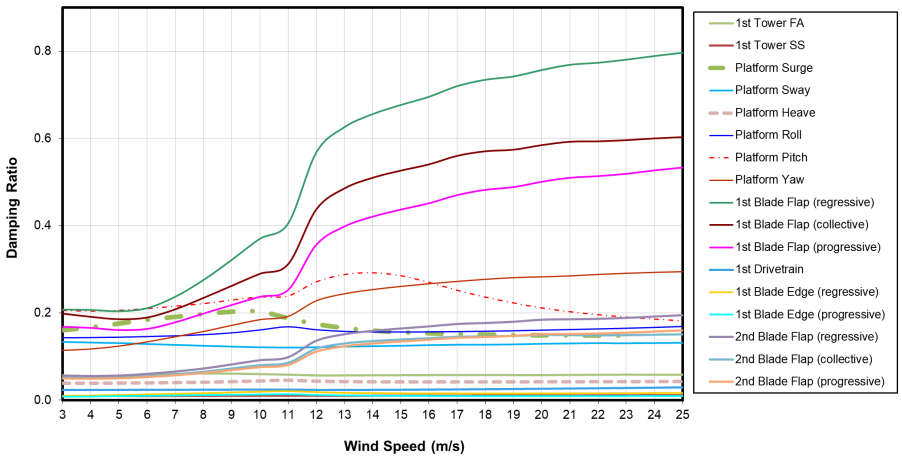

(b) FAST v7

Figure 5: Damping ratios as a function of wind speed for (a) OpenFAST and (b) FAST v7

Figure 5 shows that there are some significant differences between the damping ratios given by OpenFAST and those given by FAST v7. One of the major causes of these differences comes from enabling the "Frozen Wake" feature in the OpenFAST linearization, which was not available in the FAST v7 linearization process. This has a definite impact because it adds additional aerodynamic damping to the model. The difference between linearization with and without the frozen wake feature is described in [6], and the newer frozen wake option is expected to be more accurate. This, however, is not the only factor contributing to the differences; it may also depend on the perturbation size used as described previously. This is an open area of research and will continue beyond the work presented here.

5. State-Space Model

The state-space model method of calculating platform wave forces was compared to the standard method involving the inverse Fourier transform calculations in HydroDyn. The approximate order of the state-space models (number of states) needed for accurate wave load calculations was assessed. These results are shown for the OC4-platform [7].

For this platform model, the panel code WAMIT was used with a constant frequency resolution of 0.05 radians per second to generate data needed to determine the platform frequency-response functions (FRFs). The noncausal impulse-response functions (IRFs) were then calculated by a MATLAB script and then time-shifted to arrive at causal IRF. This time delay was set at $t_c = 10s$ for the OC4 platform. Figure 6 shows the noncausal and time-shifted causal IRFs for the OC4 platform for the surge and pitching degrees of freedom. The wave heading direction was set at zero degrees.

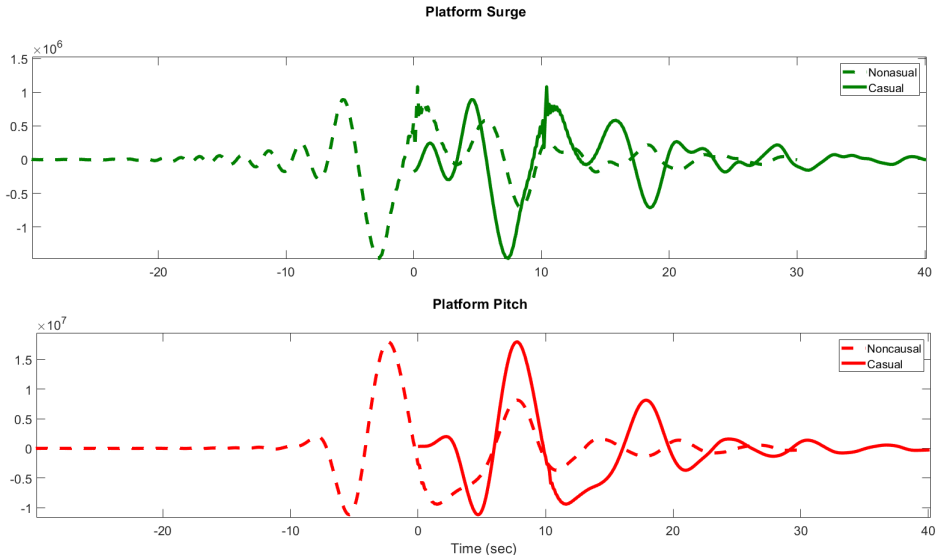

Figure 6: Noncausal and causal platform surge and pitching impulse response functions for the OC4 platform

Next, impulse responses and wave force time histories were compared between the various models. Figure 7 shows the IRF comparisons. The blue curve (X_t) represents the causal IRF to be approximated. The red curve (Y-full order) is the impulse response from a high-order fitted state-space model (approximately 400 states). The other curves represent the impulse responses from reducing the state-space models (6, 8 and 12 states) using MATLAB's balanced model reduction algorithms [8] for each load component. We can see that the 12-order state-space model does the best job of approximating the original IRF. The lower order state-space models give less accurate approximations.

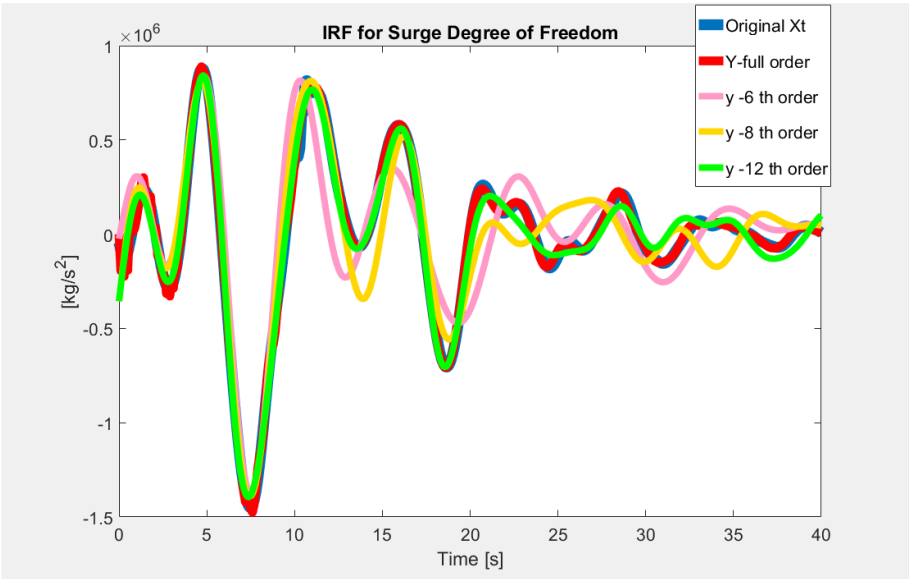

(a) Platform surge

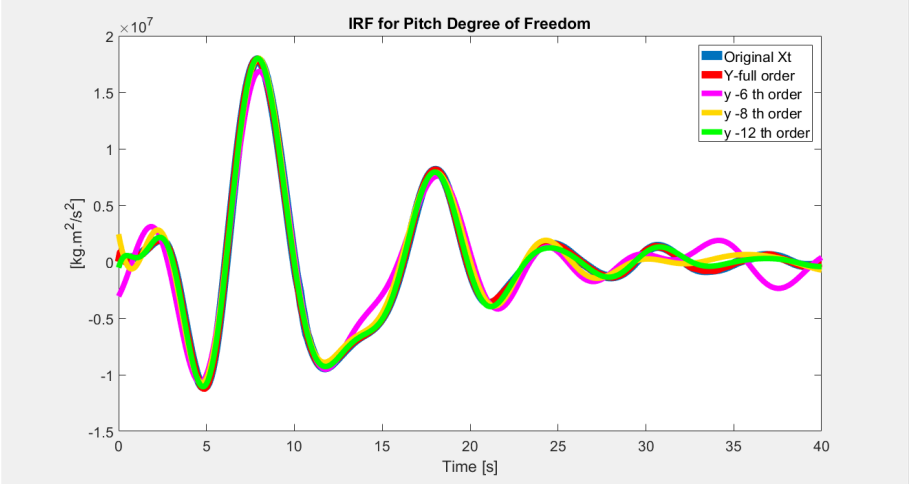

(b) Platform pitch

Figure 7: IRF approximations for platform surge and pitching degrees of freedom for the OC4 platform for (a) platform surge and (b) platform pitch

Examination of the calculated wave forces provides even more insight into the required order of the state-space models necessary for accurate wave force calculations. The calculated wave forces for the OC4 platform for a regular wave case are shown in Figure 8. The regular wave had a period of 12 s and a height of 5 m.

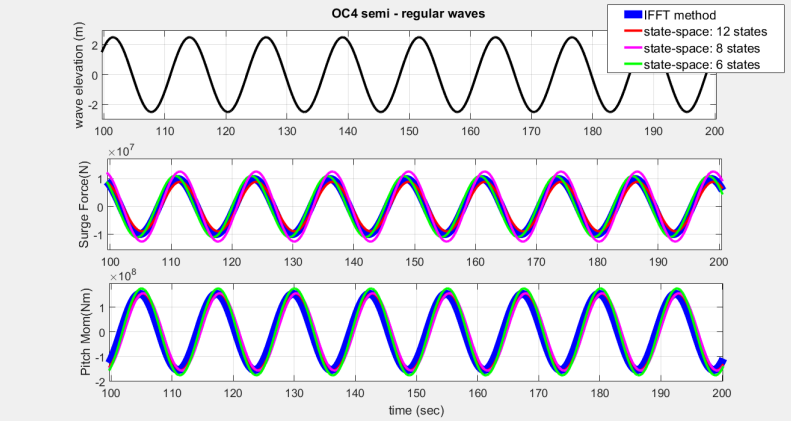

Figure 8: Comparison of wave forces calculated by the fast Fourier transform and state-space model for the OC4 regular wave case

This shows comparisons between the inverse Fourier transform wave force calculations and results from the 6-, 8-, and 12-order state models for the OC4 platform surge force and pitching moment for the regular wave case. In general, the results from the state-space models better replicate the inverse Fourier transform results as the number of states increase, with the best results from the 12-state model.

Next, this comparison is made for an irregular wave case for the same platform. This case has the same dominant wave frequency and height (12-s period, height 5 m.) as the regular wave case. Figure 9 shows the comparisons for the OC4 platform's surge force and pitching moment. In general, the state-space models gave the best results for the platform pitching moment calculation. The highest order state-space model (12 states) still had difficulty replicating the inverse fast Fourier transform results for the surge degree of freedom. This could be because of the complicated structure of the OC4 platform. The results were calculated using higher order state-space models (up to 20 states) but we found that these models gave surge force calculations that were not much different than the 12-state model. For the OC4 platform, at least a 12-state model is needed to attempt to replicate the inverse fast Fourier transform results, and even with this order of state-space models, the inverse fast Fourier transform results were replicated with only fair accuracy.

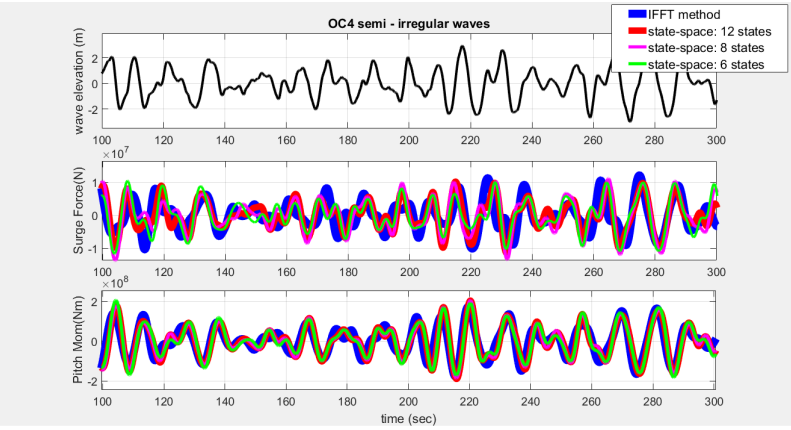

Figure 9: Comparison of wave forces calculated by the fast Fourier transform and state-space model for the OC4 semi, irregular wave case

6. Time-domain comparison between linear and nonlinear solutions

Finally, time-domain simulations of the NREL 5-MW baseline wind turbine atop the OC4 platform are run with small, moderate, and severe waves, both regular and irregular, with both the linear state-space and nonlinear time-domain models. The intent here is to show that the linearized model is capable of replicating a realistic response when given a time series of wave elevations as an input to the system.

In these results, the ElastoDyn, ServoDyn, HydroDyn, and MAP++ modules were enabled and the InflowWind and AeroDyn modules were disabled. All pertinent structural degrees of freedom were enabled in the ElastoDyn module including blade-bending, drivetrain-torsion, nacelle-yaw, tower-bending, and floating platform translation. Additionally, rotation DOFs—and gravitational loading, structural (but no aerodynamic) damping, mooring restoring, and hydrodynamic added mass, radation and viscous damping, hydrostatic restoring, and wave-excitation were included, and generator-rotation was disabled. The ServoDyn module provided nacelle-yaw actuator stiffness and damping. One linearization analysis was run at 0 rpm in still water (i.e., the wave-elevation operation point is zero, but the linear state-space model included a wave-elevation perturbation from still water as an input). A steady-state condition was found by marching the nonlinear solution in time long enough for start-up transients to die out (the start-up transients exist because gravity has an influence on the structural displacements, which are assumed undisplaced at time zero, and die out as a result of structural and hydrodynamic damping). After a steady-state condition was reached, an operation point was set and the linearized full-system matrices (A, B, C, and D) were computed. Separate nonlinear time-domain simulations were completed for small, moderate, and severe wave heights (0.67 m, 2.44 m, and 5.49 m, respectively) for regular and irregular waves at a period of (4.8 s, 8.1 s, and 11.3 s, respectively). A time series of each of the wave elevation histories from the nonlinear model were time-shifted forward by 10 s and used in the linearized model to address the noncausality of the wave forcing. The MATLAB function “lsim” was used to compute the time-domain response from the linear state-space response model, and the fixed operation point values were added to this response for proper comparison to the nonlinear response (because the solution to the state-space model is a perturbation about the operation point).

Next, simulation results from the state-space and time-domain models were compared. For each simulation, the startup transients were removed from the plots. Figure 10 shows the state-space and time-domain model response for small regular waves with a wave height of 0.67 m for platform surge, platform heave, platform pitch, and tower top fore-aft motion.

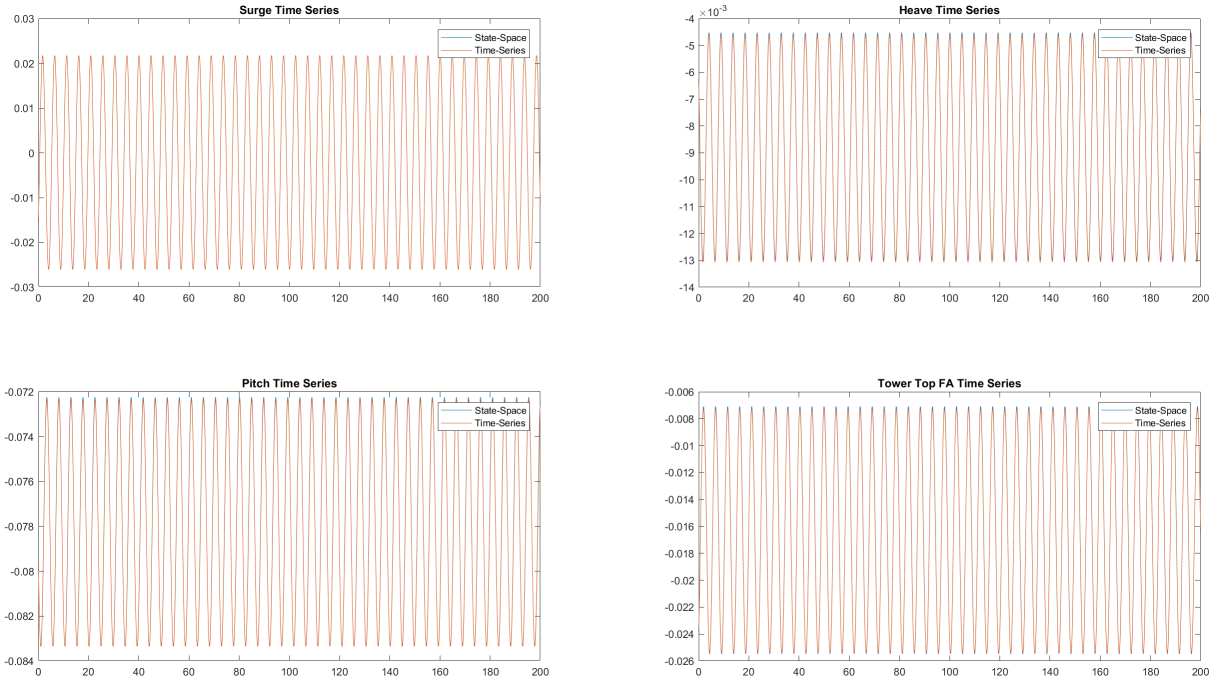

Figure 10: Platform response for regular waves with wave height = 0.67 m for both the state-space and time-domain response

Figure 11 shows the state-space and time-domain model response for small irregular waves with a wave height of 0.67 m for platform surge, platform heave, platform pitch, and tower top fore-aft motion.

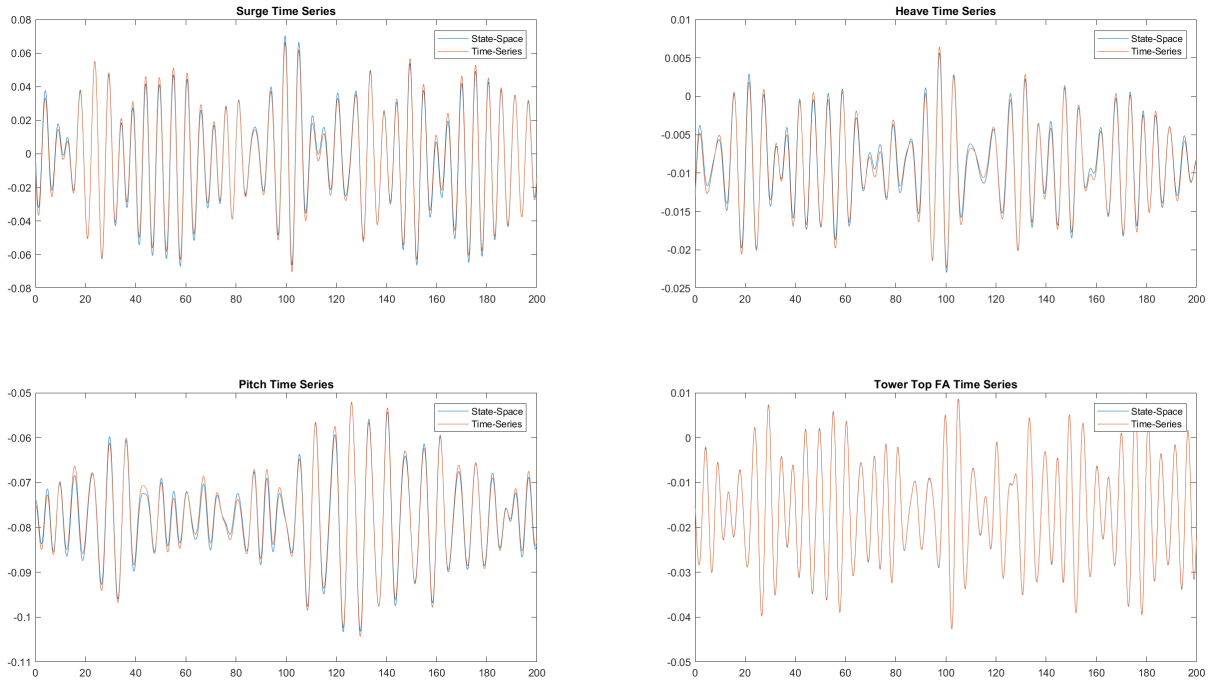

Figure 11: Platform response for irregular waves with wave height = 0.67 m for both the state-space and time-domain response

Figure 12 shows the state-space and time-domain model response for moderate regular waves with a wave height of 2.44 m for platform surge, platform heave, platform pitch, and tower top fore-aft motion.

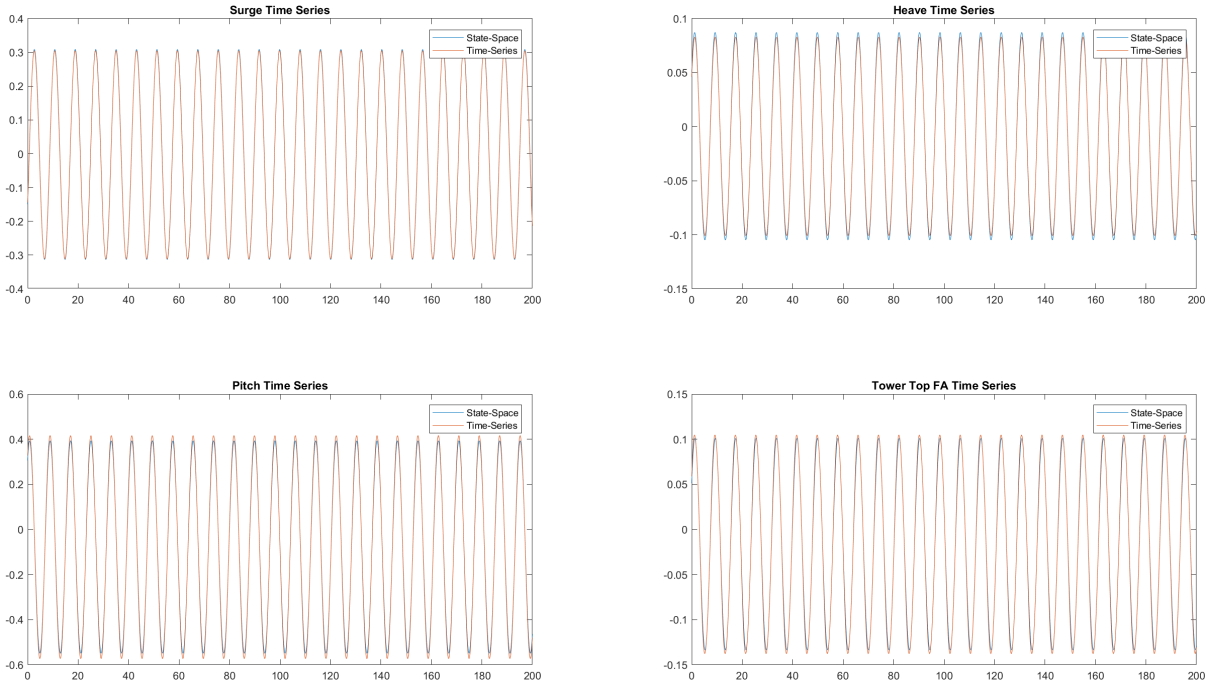

Figure 12: Platform response for regular waves with wave height = 2.44 m for both the state-space and time-domain response

Figure 13 shows the state-space and time-domain model response for moderate irregular waves with a wave height of 2.44 m for platform surge, platform heave, platform pitch, and tower top fore-aft motion.

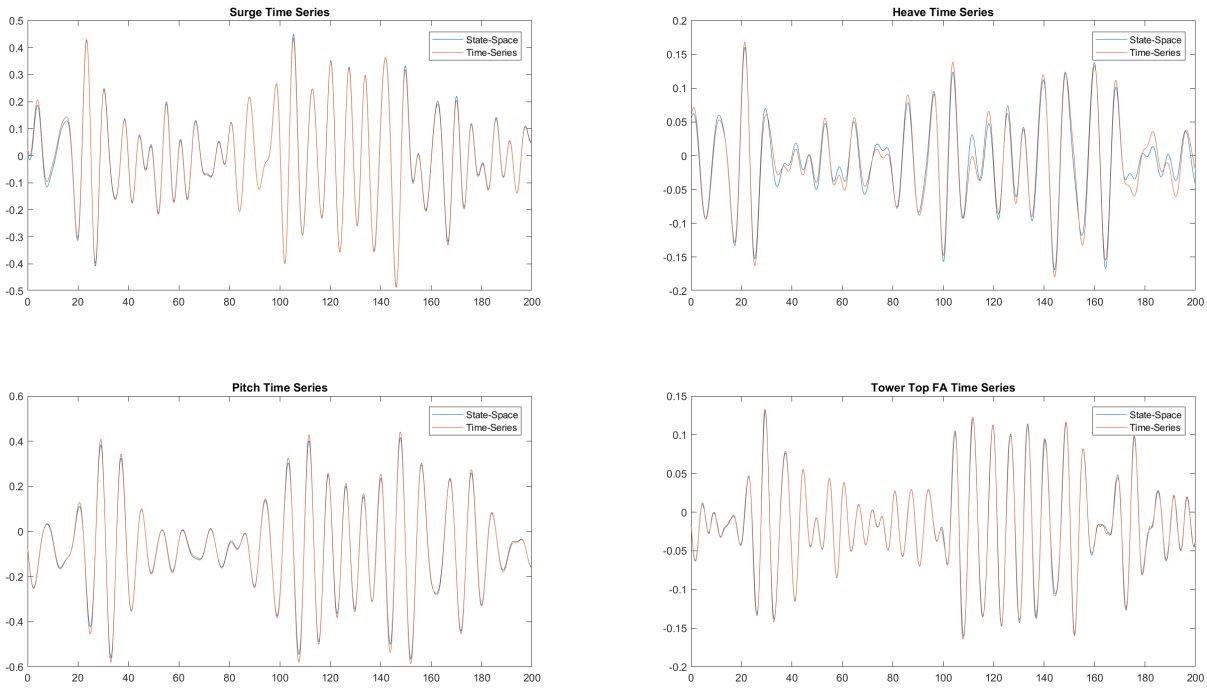

Figure 13: Platform response for irregular waves with wave height = 2.44 m for both the state-space and time-domain response

Figure 14 shows the state-space and time-domain model response for large regular waves with a wave height of 5.49 m for platform surge, platform heave, platform pitch, and tower top fore-aft motion.

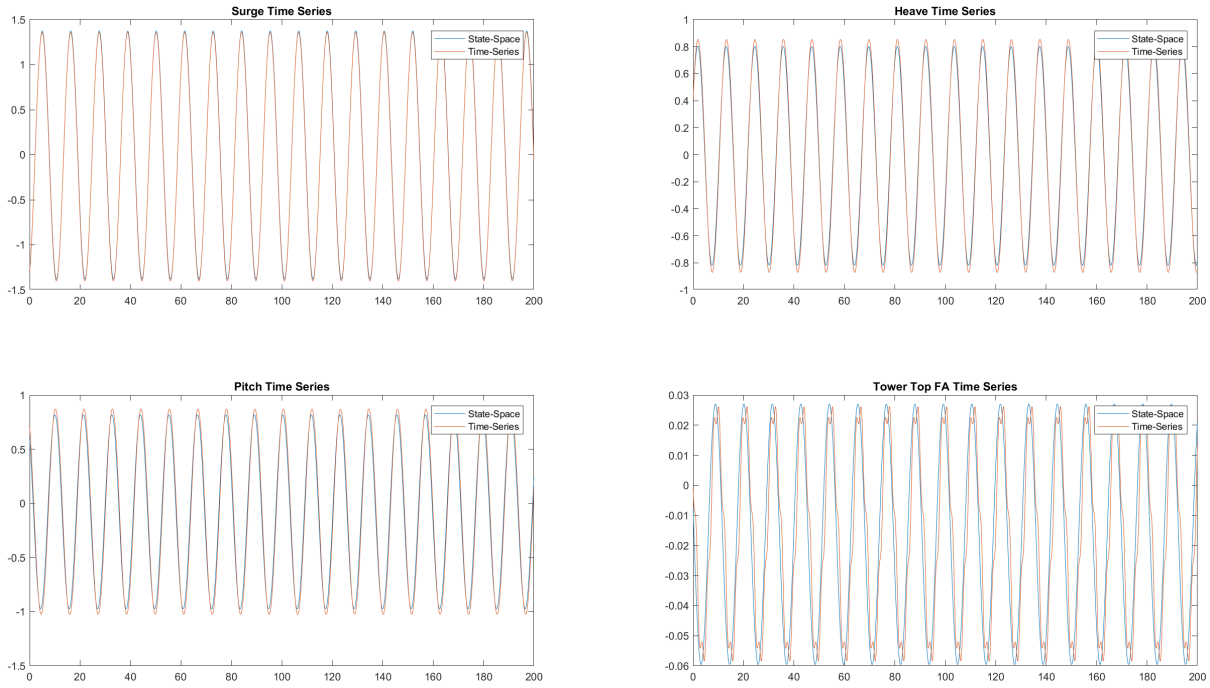

Figure 14: Platform response for regular waves with wave height = 5.49 m for both the state-space and time-domain response

Figure 15 shows the state-space and time-domain model response for large irregular waves with a wave height of 5.49 m for platform surge, platform heave, platform pitch, and tower top fore-aft motion.

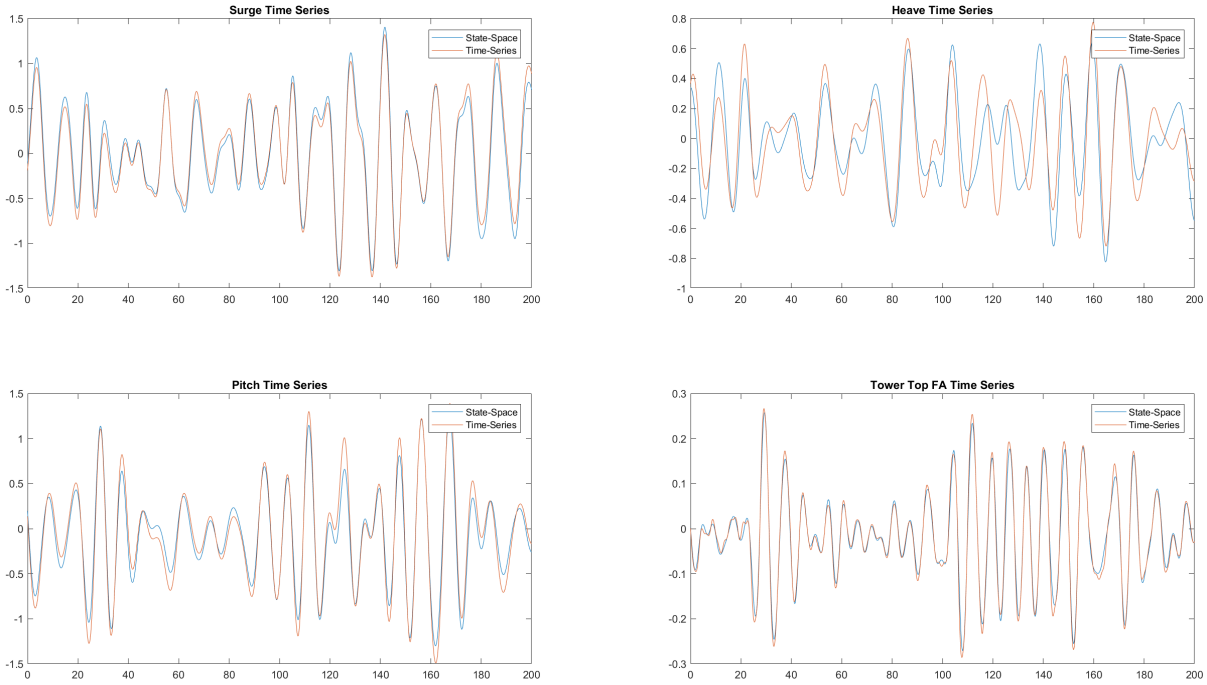

Figure 15: Platform response for irregular waves with wave height = 5.49 m for both the state-space and time-domain response

The general trends shown in Figures 10−15 suggest that there is a good match between the simulations for the linear state-space model and the nonlinear time-domain model. The state-space wave-excitation model is well tuned for the low periods associated with the small sea state, and not as well tuned for larger sea states. The discrepancy associated with larger sea states is most likely because of the greater importance in nonlinear behavior for larger excitations.

The standard deviation for platform surge, platform heave, platform pitch, and tower top fore-aft motion is shown in Figure 16.

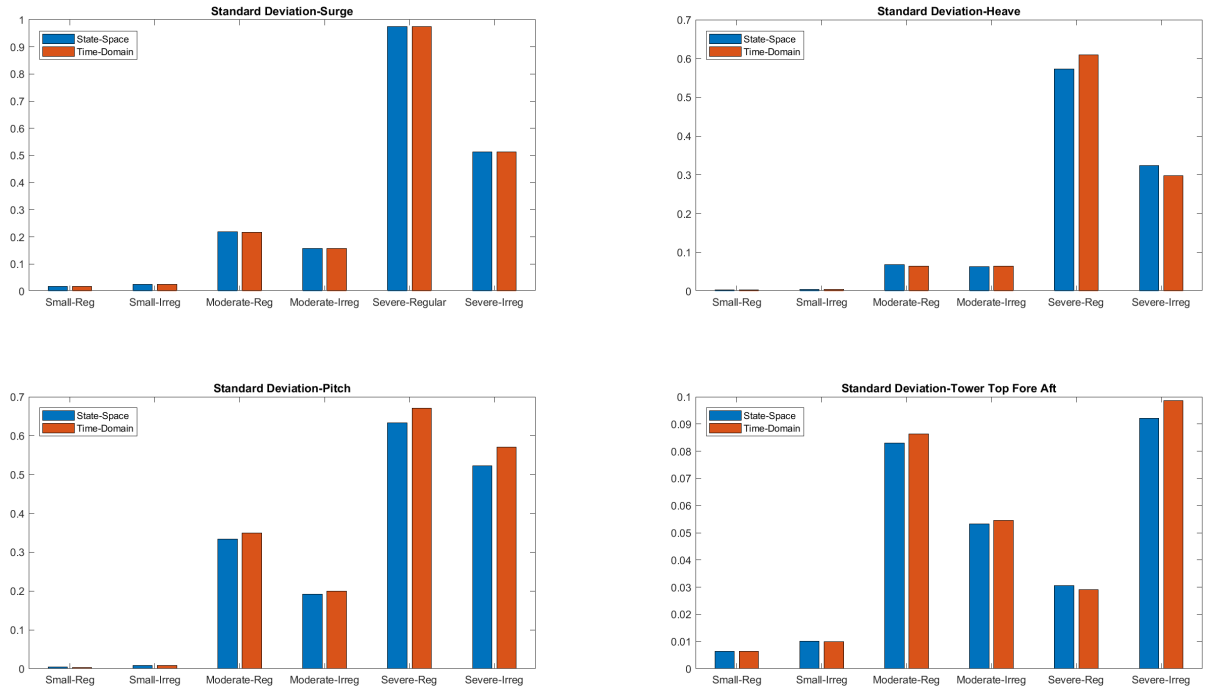

Figure 16: Standard deviation for surge for regular and irregular waves; for small, moderate, and severe wave heights; for both state-space and time-domain response

The standard deviation aligns well between the state-space and time-domain models. In general, as the wave elevation increases from small to large, the discrepancy in standard deviation increases. From the time-domain comparisons we can see that this would be expected, and there is a good fit between the state-space model and the time-domain model. The surge motion is captured very well for all sea states and has little discrepancy in standard deviation. The accuracy of the other degrees of freedom is not quite as good as the wave severity increases. This is likely a result of the linear model development and tuning of the state-space hydrodynamic models. From the standard deviation analysis, we can see that the linearization functionality of OpenFAST is yielding accurate results.

7. Conclusions

The first part of the verification comparison shows good agreement between natural frequencies and damping ratios calculated by OpenFAST and FAST v7. Some discrepancies do exist between the natural frequencies and damping ratios, which have to do with the ability to trim the solution in FAST v7, perturbation size in the respective codes, the use of the frozen wake feature in the OpenFAST linearization, as well as the influence of wave radiation on the damping, which could not be accounted for in the prior linearization capability. The wave parametric studies in OpenFAST show that comparison between the linearized and nonlinear solutions is quite good for the response behavior of a floating wind turbine, but start to deviate at more severe sea states because of the increasing importance of nonlinearites in the structural response.

Overall, we believe the new linearization functionality in OpenFAST is verified and the new features can be used with confidence. We envision that the new linearization capabilities in

OpenFAST will allow for greater insight into floating wind system dynamics and advanced controller design for floating systems in both industry and academia. Future work in the area will include further investigation into the relationship between perturbation size and damping ratio, and developing a trim solution for OpenFAST linearization.

8. Acknowledgments

This work was authored [in part] by the National Renewable Energy Laboratory, operated by Alliance for Sustainable Energy, LLC, for the U.S. Department of Energy (DOE) under Contract No. DE-AC36-08GO28308. Funding provided by the U.S. Department of Energy Office of Energy Efficiency and Renewable Energy Wind Energy Technologies Office. The views expressed in the article do not necessarily represent the views of the DOE or the U.S. Government. The U.S. Government retains and the publisher, by accepting the article for publication, acknowledges that the U.S. Government retains a nonexclusive, paid-up, irrevocable, worldwide license to publish or reproduce the published form of this work, or allow others to do so, for U.S. Government purposes.

9. References

[1] Jonkman J M, Wright A D, Hayman G J and Robertson A N 2018 Full-system linearization for floating offshore wind turbines in openfast ASME 2018 1st International Offshore Wind Technical Conference (American Society of Mechanical Engineers) pp V001T01A028–V001T01A028
[2] Bir G S 2010 User's guide to mbc3: Multi-blade coordinate transformation code for 3-bladed wind turbine Tech. rep. NREL, Golden, CO (United States)
[3] Jonkman J M 2010 Definition of the Floating System for Phase IV of OC3 (Citeseer)
[4] Jonkman J M and Buhl Jr M L 2005 Fast user's guide-updated august 2005 Tech. rep. NREL, Golden, CO (United States)
[5] Jonkman J, Butterfield S, Musial W and Scott G 2009 National Renewable Energy Laboratory, Golden, CO, Technical Report No. NREL/TP-500-38060
[6] Jonkman J M and Jonkman B J 2016 Fast modularization framework for wind turbine simulation: Full-system linearization Journal of Physics: Conference Series vol 753 (IOP Publishing) p 082010
[7] Robertson A, Jonkman J, Masciola M, Song H, Goupee A, Coulling A and Luan C 2014 Definition of the semisubmersible floating system for phase ii of oc4 Tech. rep. National Renewable Energy Lab.(NREL), Golden, CO (United States)
[8] Varga A 1991 Balancing free square-root algorithm for computing singular perturbation approximations Decision and Control, 1991., Proceedings of the 30th IEEE Conference on (IEEE) pp 1062–1065